Agricultural Water Management 116 (2013) 160–174

Contents lists available at SciVerse ScienceDirect

Agricultural Water Management

journal homepage: www.elsevier.com/locate/agwat

Simulation of furrow irrigation using the Slow-change/slow-flow equation

F. Soroush[a,*], J.D. Fenton[b], B. Mostafazadeh-Fard[a], S.F. Mousavi[a], F. Abbasi[c]

[a] Water Engineering Department, College of Agriculture, Isfahan University of Technology, Isfahan 84156-83111, Iran
[b] Institute of Hydraulic and Water Resources Engineering, Vienna University of Technology, Karlsplatz 13/222, 1040 Vienna, Austria
[c] Agricultural Engineering Research Institute, Karaj, Iran

ARTICLE INFO

Article history:
Received 3 March 2012
Accepted 19 July 2012
Available online 10 August 2012

Keywords:
Numerical model
Infiltration
Hydraulic resistance
Evaluation

ABSTRACT

A furrow irrigation model is developed based on the Slow-change/slow-flow routing equation, which is an approximate reduced form of the Saint-Venant equations to a single equation with a single variable, the upstream volume of water. For downstream-propagating disturbances it can be shown that the only approximation is that the rate of change of upstream inflow is small, with no limit on Froude number, so that it can be used for all slopes. It can also be used with all common end conditions. To calculate resistance to flow a composite model in terms of almost any boundary roughness is proposed. Infiltration is assumed to follow the Kostiakov formula. The equation was solved numerically using explicit Euler and implicit Crank–Nicolson schemes. Seven furrow-field data sets were used to verify the model simulation of advance and recession trajectories and runoff. In all cases examined, the model predictions were in good agreement with field data and results from existing software. The proposed model can provide a suitable and simple numerical simulation tool for design and evaluation of furrow irrigation for all bottom slopes and boundary conditions.

1. Introduction

Surface irrigation is the oldest and most widely used method for irrigating agricultural lands across the world. Surface irrigation systems are characterized by their operational simplicity and their complicated analysis and design. The numerical analysis of surface irrigation systems started in the 1970s, aiming at optimizing design and management by maximizing the insight obtained from resource-consuming field experiments (Burguete et al., 2009). The Saint-Venant long wave equations, which include a mass conservation equation and a momentum equation, are a good model of furrow and overland flow conditions in surface irrigation. Several studies have utilized the full equations or their simplified forms in hydraulic modeling of surface irrigation or some aspects thereof (Bassett and Fitzsimmons, 1976; Fangmeier and Strelkoff, 1979; Sherman and Singh, 1982). Mathematical models of furrow irrigation processes can be generally classified, after Walker and Humpherys (1983), in decreasing accuracy of approximation as:

(a) Hydraulic models, using the full long-wave (Saint-Venant) equations. These have the potential to be most accurate in predicting flow conditions in surface irrigation problems. However, due to the complexity of current numerical methods required to solve the full equations, reduced forms of the models, such as the Zero-inertia and the Kinematic-wave models, have been developed to simulate irrigation flow.
(b) Zero-inertia models were introduced for border and basin irrigation by Strelkoff and Katopodes (1977a), and applied to furrow irrigation by Elliott et al. (1982). The Zero-inertia model was originally stated to be based on the assumption that some terms in the momentum equation are proportional to the square of the Froude number, which are negligible in most flow conditions of surface irrigation. USDA-ARS (2009) stated that it is applicable to all practical field conditions.
(c) Kinematic-wave models for relatively steep slopes (Walker and Humpherys, 1983). The kinematic-wave model is based on a further approximation that the surface slope deviates little from the bed slope. It is supposed to be limited to relatively large slopes and cannot handle any downstream boundary conditions that affect upstream flow.
(d) Volume balance models neglect the entire momentum equation and implement some approximations to the continuity equation (Walker and Skogerboe, 1987).

Fenton (2012) has shown that the customary assumptions behind the Zero-inertia approximation to the momentum equation are questionable, even if the approximation itself is a good one. In the theory leading to the Zero-inertia model, the time derivative term in the full momentum equation is scaled with respect to velocity, such that it appears to be an inertial term and is deleted

* Corresponding author. Tel.: +98 311 391 7091; fax: +98 311 391 2254.
E-mail address: f.soroush@ag.iut.ac.ir (F. Soroush).

0378-3774/$ – see front matter © 2012 Elsevier B.V. All rights reserved.
http://dx.doi.org/10.1016/j.agwat.2012.07.008

along with other inertial terms. Fenton (2012) showed that the magnitudes of the deleted terms are actually related to the time scale of change of input to the system and that it is actually an approximation based on slow-change in the channel. The model is accurate for downstream propagating long waves with no limitation on Froude number, and hence none on downstream slope. For upstream propagating waves, such as those caused by gate movements downstream, there is still a requirement that the Froude number be not too large. In accordance with these results we will refer to the simplified momentum equation, not as the Zero-inertia equation, but as the Slow-change/slow-flow momentum equation: slow-change for downstream propagation and both slow-change and slow-flow for upstream propagation. In this paper we consider mostly upstream changes propagating downstream, so there is no requirement here that the flow be slow. We will continue to use the generic name.

In fact, in furrow irrigation problems the boundary changes are often not applied slowly, and the most important approximation will be violated. However Fenton et al. (1999), while still believing that their model was a low-inertia model, showed that the model agreed well with numerical solutions of the long wave equations at almost all times, except in the vicinity of rapid changes of input, but strangely, that the subsequent results seemed to have little memory of those times of disagreement.

Another deduction by Fenton (2012) was that the kinematic wave approximation is most accurate in the limit of very long waves. However, it is an approximation that is not necessary to make unless one wants a simplified equation and computational methods. In general its results should be able to be described by the Slow-change/slow-flow equation and it is not entirely clear why some models prefer to switch to that for steeper slopes.

A useful step is the introduction of the concept of the total volume upstream of a point in space and time. This quantity satisfies the mass conservation equation identically, and using it in the Slow-change/slow-flow momentum equation leads to a single equation in a single unknown, which can be used for simulation purposes. It is referred to here as the Slow-change/slow-flow routing equation. In the original presentations of the equation (Fenton et al., 1999; Fenton and Keller, 2001) used for simulating flows in rivers and canals, it was incorrectly believed to be a low-inertia model. It was also used for modeling of phosphorus transport in a surface irrigation drain (Barlow et al., 2006), where its ability to simulate flow at very small depths was an advantage. Cross-sectional area and discharge can also be specified in terms of derivatives of upstream volume, that leads to a convenient and general treatment of different upstream and downstream boundary conditions.

This paper presents a modification of the Slow-change/slow-flow routing equation for modeling of different phases of furrow irrigation based on explicit and implicit finite-difference formulations. The equation was solved initially by the explicit Euler method to maintain a numerical approach as simple as possible, but the time step size is limited because there is a definite value beyond which the scheme is unstable. An implicit Crank–Nicolson scheme was developed, allowing much larger time steps. The model was verified with some furrow irrigation field data and the results are compared with predictions of the solution model of WinSRFR (Bautista et al., 2009).

2. The governing equations

2.1. The differential equation – the Slow-change/slow-flow routing equation

The equations used are based on the one-dimensional long wave equations for a channel, using the integrated quantities of cross-sectional area of flow A and volume flow rate Q. The mass conservation equation is

$$\frac{\partial A}{\partial t} + \frac{\partial Q}{\partial x} = i, \tag{1}$$

where i is the distributed inflow into the channel per unit length of channel, x is distance along the channel, and t the time. The common approximation to the momentum equation is used:

$$\frac{1}{B}\frac{\partial A}{\partial x} + \frac{Q^2}{K^2} - \tilde{S} = 0, \tag{2}$$

where B is water surface width, K is conveyance, $\tilde{S}$ is mean downstream bed slope at a section averaged around the perimeter. The terms that have been neglected include a time derivative $\partial Q/\partial t$ and a space derivative $\partial Q/\partial x$. Fenton (2012) showed that both terms actually scale like the rate of change of input to the system, relative to the slope and resistance terms. Traditionally, it was believed that the terms scale like the square of the Froude number, leading to appellations such as “Zero-inertia”.

Now the two conservation equations in A and Q are reduced to a single equation in terms of a single dependent variable, the total volume of water V in a channel upstream of a point x at time t, which satisfies the mass conservation equation (1) identically. It can be written as a volume integral:

$$V(x,t) = \int_{x_0}^{x} A(x',t)dx', \tag{3}$$

where x_0 is the initial point, and x' is a dummy variable of integration. From the fundamental theorem of calculus,

$$\frac{\partial V}{\partial x} = A, \tag{4}$$

thus relating cross-sectional area to V.

Discharge can also be simply related to V. The time rate of change of upstream volume at a point (x, t) is

$$\frac{\partial V}{\partial t} = I - Q, \tag{5}$$

where $I(x, t)$ is the net volume rate at which the fluid is entering the channel upstream of the point and $Q(x, t)$ is the rate at which fluid volume is passing the point, thereby becoming no longer “upstream”. The term $I(x, t)$ may consist of contributions such as inflow $Q(x_0, t)$ at the upstream end of the reach considered, and distributed inflow into the channel of i per unit length of channel, which in the case of infiltration into the ground would be negative. The term is written as

$$I = Q(x_0,t) + \int_{x_0}^{x} i(x',t)dx' \tag{6}$$

In the previous presentations of this concept (Fenton et al., 1999; Fenton and Keller, 2001; Barlow et al., 2006) the contribution of inflow $Q(x_0, t)$ at the upstream end was included differently, not as consistently as this. Substituting Eqs. (4)–(6) into the mass conservation equation (1) gives:

$$\frac{\partial}{\partial t}\left(\frac{\partial V}{\partial x}\right) + \frac{\partial}{\partial x}\left(Q(x_0,t) + \int_{x_0}^{x} i(x',t)dx' - \frac{\partial V}{\partial t}\right) = i, \tag{7}$$

and performing the differentiations shows that it is satisfied identically. Solving the approximate momentum equation (2) for Q and substituting into Eq. (5) gives:

$$\frac{\partial V}{\partial t} = I - K(V_x)\sqrt{\tilde{S} - \frac{V_{xx}}{B(V_x)}}, \tag{8}$$

which is a partial differential equation for V that describes the propagation of disturbances in channels. The symbols $V_x = \partial V/\partial x$, and

$V_{xx} = \partial^2 V/\partial x^2$ are used. As well, $K(V_x)$ and $B(V_x)$ show that both are functions of V_x, the area. It has been proposed above to call Eq. (2) the Slow-change/slow-flow momentum equation; henceforth Eq. (8) will be called the Slow-change/slow-flow routing equation. It contains no approximation as to the size of disturbance, but it can be shown for small disturbances by linearizing about a uniform flow that the equation has an advection–diffusion nature.

2.2. Modification for furrow irrigation problems

Irrigation channels are effectively prismatic, with a well-defined bed slope, constant around a section, so mean downstream bed slope can be written as $\tilde{S} = S_0$ (which might still be a function of x). Infiltration from furrows is the most important component of the net outflow, and because we have defined i to be channel inflow, infiltration is expressed with a minus sign as $i = -dZ/d\tau$, where Z is infiltration volume per unit length of furrow, taken to be positive, and $\tau = t - t_a$ is intake opportunity time, t is elapsed time, and t_a is advance time of the water front to a point x along the channel. The differential equation (8) can be written as:

$$\frac{\partial V}{\partial t} = Q(x_0, t) - \int_{x_0}^{x} \frac{dZ}{d\tau} dx' - K(V_x)\sqrt{S_0 - \frac{V_{xx}}{B(V_x)}}, \tag{9}$$

in which V is the unknown dependent variable.

2.3. Infiltration

A simple power function (Kostiakov, 1932 or Kostiakov–Lewis equation) has been used to describe infiltrated water volume per unit length of furrow:

$$Z = k\tau^a + b\tau \tag{10}$$

where Z is infiltration volume per unit furrow length and k, a and b are empirical constants (b is set to zero in Kostiakov's formula). The estimation of infiltration function parameters was done by the Merriam–Keller procedure of the WinSRFR software which is a method for estimating the infiltration depth profile from a post irrigation mass balance (Merriam and Keller, 1978). The accuracy of the estimated parameters can be verified via simulation. A trial and error approach needs to be used to determine the combination of parameters (the given a and the resulting k) that will most closely reproduce the observed advance and recession trajectories, and the observed runoff hydrograph (Bautista et al., 2009).

2.4. Flow resistance

The Gauckler–Manning equation or the Weisbach–Chézy equation can be used to determine the conveyance:

$$K = \sqrt{\frac{8g}{\lambda}\frac{A^3}{W_p}} = \frac{1}{n}\frac{A^{5/3}}{W_p^{2/3}}, \tag{11}$$

where λ is the dimensionless Weisbach resistance factor, n is Manning's resistance coefficient and W_p is wetted perimeter.

The conveyance K can be calculated explicitly from the furrow cross section, in terms of A and W_p. Power law relationships can be used to characterize the furrow shape:

$$B = Ch^m \tag{12}$$

where h is depth of water, B is top width of water and C and m are constants. The geometric relationships for such furrows can be calculated based on the procedure described in Strelkoff and Clemmens (2000).

In this paper a new resistance model is proposed to calculate the flow resistance coefficient. It is a composition of the shallow water resistance equation (14) of Pagliara et al. (2008) for very shallow flows, $0.26 \le \text{Depth/Roughness} \le 5$ and equation (30) of Yen (1991) for deeper flows, $\text{Depth/Roughness} \ge 20$, neglecting Reynolds number effects. The current model used $S_0 = 0$ in the model of Pagliara et al. (2008) model as an approximation to the relatively mild slopes found in irrigation furrows, and utilized the logarithmic matching function of Guo (2002) for bridging between the two logarithmic functions. The proposed model can be written as:

$$\sqrt{\frac{8}{\lambda}} \approx 4.26 + 3.04 \ln\frac{A/W_p}{d_{84}} - 0.295 \ln\left(1 + \left(\frac{1}{22}\frac{A/W_p}{d_{84}}\right)^2\right), \tag{13}$$

valid for a very wide range of Depth/Roughness $(A/W_p)/d_{84} \ge 0.26$, particularly useful for the commencement of irrigation when the depth is small.

In the case of using the Gauckler–Manning equation, the Manning resistance coefficient can be obtained from this by solving Eq. (11) for n:

$$n = \sqrt{\frac{\lambda}{8g}}\left(\frac{A}{W_p}\right)^{1/6}. \tag{14}$$

Strickler's formula for n in terms of relative roughness could be used, but more experimental evidence is required for Eq. (13).

3. Initial and boundary conditions and applicability to slow and fast flows

3.1. Initial condition for furrow irrigation

In many irrigation problems, at first there is no flow in the furrow. Therefore, initial conditions are zero cross-section initially, and $V(x, 0) = 0$ for all x. For computational purposes, however, it was necessary to assume a small initial depth of 2 mm in the furrow.

Eq. (9) describes the surface and subsurface water profiles as the irrigation stream first advances in the furrow, then reaches the end of the field and runs off, and finally recedes from the field after the upstream inflow is terminated.

Two assumptions were used in the program to estimate advance and recession times:

(1) Advance time was taken to be the time, t_x at which flow depth at a particular point of x first exceeds 2 mm; (2) recession was presumed to occur at a particular point and time after the cutoff time when flow depth at that point dropped below 2 mm.

3.2. Boundary conditions

3.2.1. Upstream point x_0

The volume of water upstream of $x = x_0$ is indeed always zero, such that $V(x_0, t) = 0$ for all t, suggested by Eq. (3). Whereas this is simple, the details of the inflow history $Q(x_0, t)$ are included in the governing differential equation (9).

3.2.2. Downstream boundary

In many situations in surface irrigation, it is assumed that there is no control at the end of a furrow. This is an open boundary condition, which can be approximated by a uniform flow, giving discharge as a function of surface elevation. In some furrow irrigation applications there is a flume or control structure at the downstream end. We generalize to allow for all common cases, expressing the relationship between flow and surface elevation, the downstream boundary condition, as:

$$Q_n = \phi(h_n), \tag{15}$$

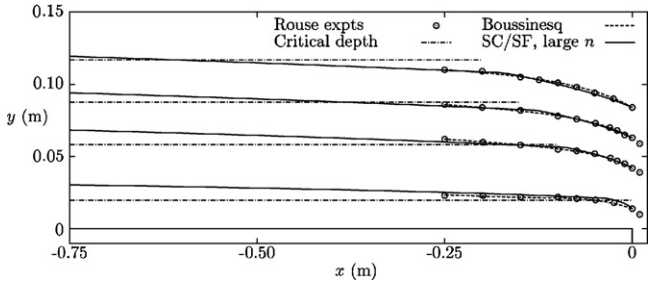

Fig. 1. Free overfall – Rouse's experimental results, critical depths, numerical solutions of the Boussinesq equation, and numerical solutions of the Slow-change/slow-flow momentum equation for artificially high n for a distance of two depths to simulate the overfall.

where n is the index of the end point, $\phi()$ is given by the surface-elevation-discharge characteristic of the uniform flow or outflow structure. For our purposes immediately below it is simpler to express it not in terms of surface elevation but as a function of the channel depth h_n at the end. The function will possibly also be determined by other quantities independent of the flow such as the channel bed elevation, the crest elevation of a weir, and so on. From the cross-sectional geometry, water depth can be written as a function of cross-sectional area, $h_n = \psi(A_n)$, such that, in terms of V:

$$h_n = \psi\left(\left.\frac{\partial V}{\partial x}\right|_n\right) \tag{16}$$

The downstream boundary condition for the end point can now be written, in the spirit of the differential equation (9), but where the flow past the point is expressed, not in terms of conveyance and local slope as in the interior of the channel, but in terms of Q_n using Eqs. (15) and (16):

$$\left.\frac{\partial V}{\partial t}\right|_n = Q(x_0, t) - \int_{x_0}^{x_n} \frac{dZ}{d\tau} dx' - \phi\left(\psi\left(\left.\frac{\partial V}{\partial x}\right|_n\right)\right) \tag{17}$$

3.2.3. The free overfall

There is another boundary condition, the free overfall, which is relatively rare, but we consider it here because it has received some unsatisfactory treatment in the past. It is where a channel flow passes over a sudden brink at the end, rather like a waterfall. Of course, good irrigation practice might try to avoid such an occurrence, where loss of water from the channel and loss of head anywhere are best avoided. The flow in the channel might be sub- or super-critical, but before it passes over the brink the free surface starts to curve appreciably downwards, such that the pressure distribution is no longer hydrostatic, the long-wave equations cannot be applied, and they cannot describe the possible passage between sub- and super-critical flow. The flow is also fast enough that the inertia terms in the equations are important. This would seem to rule out the Zero-inertia approximation. However, as described above, Fenton (2012) suggested that the equation is actually a slow-change approximation and can be used for large Froude numbers. However, the appreciably curved streamlines and non-hydrostatic pressure should rule it out for the free overfall problem. Nevertheless, we explored the use of the slow-change momentum equation also for that problem. We simulated the experimental results of H. Rouse from his PhD thesis presented in the first chapter of his selected works by Kennedy and Macagno (1971). Fig. 1 shows four experimental surface profiles shown by circles plus horizontal chain-dashed lines showing the critical depth. It can be seen that the upstream flow was sometimes sub-, sometimes super-critical, but in each case it passed over the brink with a depth less than critical. To simulate the problem including the effects of curvature we first used a Boussinesq momentum equation, which included inertial terms plus a third derivative of elevation. The results are shown by a dashed line, and approximate the experimental points well. However the numerical solution method was non-trivial. For practical purposes, where the figure shows that the region of appreciable curvature is limited to a horizontal distance of only two water depths, we wanted to explore the use of the slow-change approximation, the subject of this work. To simulate the curved region we used an artificially high value for Manning's resistance coefficient of $n = 0.06$ for a distance of two brink depths and thereafter $n = 0.03$, both chosen so as to agree best with experimental points. Both are much larger than the real resistance of the smooth channel. This approach is not fundamental, but it shows how this difficult problem can be simulated over a very short length of channel using our present approximation.

Our recommended procedure for the relatively rare case of a free overfall is then:

1. Calculate the brink depth h_b from the formulae presented by Beirami et al. (2006) or from other research on the problem, which all seems consistent. For example, for a rectangular section, $h_b \approx 0.7 h_c$, where critical depth $h_c = \sqrt[3]{q^2/g}$, where q is the discharge per unit width in the overfall.
2. Apply the Slow-change/slow flow equation (8) in the channel, but close to the brink, use an artificially enhanced value of resistance to simulate, albeit irrationally, the curvature of the overfall.

We note that this section contradicts most of the assertions and computational results of Strelkoff and Katopodes (1977b), who stated that the end depth was at critical $h_b = h_c$, whereas it is actually about 70% of that, and in any case the concept of criticality breaks down in a region of finite curvature; they applied the long-wave equation from the brink where their depth was critical, such that the water surface was initially vertical thereby invalidating the use of the equation; similarly they applied the Zero-inertia equation from the brink but where they asserted that the control depth was zero, so that it too gave an initially vertical surface, also invalidating the use of the equation.

3.3. Applicability to slow, transitional, and fast flows

Our application of the Slow-change/slow flow equation to the problem of the free overfall raised some general points. The equation does not contain gravity g, and so any considerations of critical depth, and sub- or super-criticality are irrelevant to it. Its apparent lack of limitation by Froude number means that it seems to be able to be used both in flows that are actually sub- and super-critical according to classical hydraulics, but where they are generally slowly varying. It could never be used for a sudden transition from super-critical to sub-critical such as a hydraulic jump, but it seems to be able to be used, albeit only as a computational approximation, in transitions in the other direction, from sub- to super-critical flow. Interestingly, the solutions shown in Fig. 1 by numerically solving it as an ordinary differential equation were all obtained by computing in an upstream direction – in the super-critical regions, in the transition regions through critical depth and in the sub-critical regions, thus violating some of the basic principles of such computations using the long-wave equations.

4. Computational schemes

4.1. Forming time-stepping schemes

The numerical solution of the differential equation (9) at $(x, t+\Delta)$ can be written as:

$$V(x, t+\Delta) = V(x, t) + \delta V_1 + \delta V_2 + \delta V_3, \tag{18}$$

where

$$\delta V_1 = \int_t^{t+\Delta} Q(x_0, t')dt', \tag{19}$$

$$\delta V_2 = -\int_{x_0}^{t+\Delta} \int_{x_0}^{x} \frac{dZ}{d\tau} dx' dt', \tag{20}$$

where Z is a function of opportunity time τ, such that:

$$\tau = \begin{cases} t - t_a & \text{if } t \geq t_a \\ 0 & \text{if } t < t_a \end{cases}, \tag{21}$$

and

$$\delta V_3 = -\int_t^{t+\Delta} K(V_x)\sqrt{S_0 - \frac{V_{xx}}{B(V_x)}}dt'. \tag{22}$$

The individual terms are approximated as follows:

Upstream inflow term: The integral for δV_1 in Eq. (19) can be evaluated by the trapezoidal rule:

$$\delta V_1 \approx \frac{\Delta}{2}(Q(x_0, t) + Q(x_0, t+\Delta)). \tag{23}$$

Infiltration term: The integral of the second term (infiltration) is a little more difficult. The infiltration derivative is commonly infinite at the commencement of infiltration. The two sets of limits of integration are independent of each other. So, the difficulty of infinite infiltration can be overcome by reversing the order of integration:

$$\delta V_2 = -\int_{x_0}^{x} (Z(t+\Delta - t_a(x')) - Z(t - t_a(x')))dx'. \tag{24}$$

The Kostiakov equation (10) is substituted into Eq. (24) and then the integrand is expanded as a power series in Δ for a first-order approximation of the integrand. The final approximation is evaluated using the trapezoidal rule to integrate from x_0 to x_j, where j is the point under consideration:

$$\delta V_2 \approx -k\delta x \sum_{m=0}^{j}{}'' \left(\left[t + \Delta - t_a(x_m)\right]^a - \left[t - t_a(x_m)\right]^a \right), \tag{25}$$

where δx is the space step, and summation over m includes factors of 1/2 at the end points $m = 0$ and j, which is indicated by the double prime superscript $\sum''$ and where the square brackets [] are such that if the quantity inside is less than zero, the result is zero.

Gravity-resistance term: The simplest but least accurate explicit time-stepping scheme for Eq. (22) is the Euler method, where the integrand is approximated over the whole step by the value at time t at the beginning of the step:

$$\delta V_3 = -\Delta K(V_x)\sqrt{S_0 - \frac{V_{xx}}{B(V_x)}}\Bigg|_t \tag{26}$$

A more accurate and stable scheme is to use the Crank–Nicolson or trapezoidal approximation and write it as:

$$\delta V_3 = -\frac{\Delta}{2}\left(K(V_x)\sqrt{S_0 - \frac{V_{xx}}{B(V_x)}}\Bigg|_t + K(V_x)\sqrt{S_0 - \frac{V_{xx}}{B(V_x)}}\Bigg|_{t+\Delta} \right). \tag{27}$$

In the second term, to be evaluated at $t+\Delta$, the spatial derivatives include other, as yet unknown, values of V at $t+\Delta$, and the scheme is implicit.

4.2. First-order explicit time-stepping

4.2.1. Computational scheme at inner points

The simplest explicit time-stepping scheme to solve Eq. (9) numerically is equivalent to Euler's method for solving ordinary differential equations:

$$V(x_j, t+\Delta) = V(x_j, t) + \Delta \left.\frac{\partial V}{\partial t}\right|_j + O(\Delta^2), \tag{28}$$

which, using Eqs. (9), (18) and (26), gives

$$V(x_j, t+\Delta) = V(x_j, t) + \delta V_1(x_j, t) + \delta V_2(x_j, t) - \Delta K(V_x)\sqrt{S_0 - \frac{V_{xx}}{B(V_x)}}\Bigg|_t, \tag{29}$$

where δV_1 is given by Eq. (23) and δV_2 by Eq. (25). This scheme is simple, but has limited numerical properties as it is explicit, and does not attempt to build in the wave like nature of solutions of the equation, as compared with the upwinding schemes developed by Barlow et al. (2006). The first and second space derivatives in Eq. (29) were approximated by assuming a uniform partition in space and using three-point formulae. An alternative for the approximation of space derivatives was the implementation of cubic splines using "not-a-knot" boundary conditions at the ends (De Boor, 1978).

4.2.2. Downstream boundary condition

The last equation in the explicit scheme is given by considering Eq. (17) for the downstream boundary condition at $j = n$:

$$V_n^{i+1} = V_n^i + \delta V_1(x_n, t) + \delta V_2(x_n, t) + \Delta\left(\phi\left(\psi\left(\left.\frac{\partial V}{\partial x}\right|_n^i\right)\right)\right), \tag{30}$$

where $\phi()$ is the function for flow in terms of depth as given in Eq. (15) and $\psi()$ is the function for depth in terms of cross-sectional area given by Eq. (16). A one-sided three-point finite difference approximation for the derivative was used.

4.3. Second-order implicit time-stepping (Crank–Nicolson)

4.3.1. Computational scheme at inner points

Second order implicit time-stepping can be expressed by collecting contributions of Eqs. (9), (18) and (27):

$$V(x_j, t+\Delta) = V(x_j, t) + \delta V_1(x_j, t) + \delta V_2(x_j, t) - \frac{\Delta}{2}\left(K(V_x)\sqrt{S_0 - \frac{V_{xx}}{B(V_x)_{(x_j,t)}}}\Bigg| + K(V_x)\sqrt{S_0 - \frac{V_{xx}}{B(V_x)}}\Bigg|_{(x_j,t+\Delta)} \right), \tag{31}$$

where δV_1 is given by Eq. (23) and δV_2 by Eq. (25). An implicit Crank–Nicolson scheme, based on this trapezoidal rule in time, was used to numerically solve Eq. (31). Bringing all terms to the left side and discretizing the x-derivatives by central three-point approximations, using the convention of i and j for time and distance indices respectively leads to a non-linear equation in terms of the three unknowns V_{j-1}^{i+1}, V_j^{i+1}, and V_{j+1}^{i+1}.

4.3.2. Downstream boundary condition

The last equation in the Crank–Nicolson scheme is given by considering Eq. (17) for the downstream boundary condition at:

$$V_n^{i+1} - V_n^i - \delta V_1(x_n, t) - \delta V_2(x_n, t) + \frac{\Delta}{2}\left(\phi\left(\psi\left(\left.\frac{\partial V}{\partial x}\right|_n^{i+1}\right)\right) + \phi\left(\psi\left(\left.\frac{\partial V}{\partial x}\right|_n^{i}\right)\right)\right) = 0, \quad (32)$$

where $\phi()$ is the function for flow in terms of depth, as given in Eq. (15) and $\psi()$ is the function for depth in terms of cross-sectional area given by Eq. (16). One-sided three-point finite difference approximations for the derivatives were used.

4.3.3. Solving the system of equations

The implicit Crank–Nicolson scheme, which is unconditionally stable under most circumstances, solves the resulting set of equations simultaneously for all computational points at each time step. The system is composed of Eq. (31) at each interior point and Eq. (32) at the last point. It can be written as:

$$f_l(V_j^{i+1}, j = 1, \ldots, n) = 0 \quad \text{for} \quad l = 1, \ldots, n \quad (33)$$

As the partial differential equation is non-linear, discretization of Eqs. (31) and (32) will also be non-linear so that advancing in time will involve solution of a system of non-linear algebraic equations. Newton's method as a generalized gradient method was used to develop an iteration scheme to solve the system of non-linear equations. The related matrix is tri-diagonal, and can be solved by the Thomas Algorithm (Thomas, 1949).

A simpler method is to use direct iteration at each point. As $f_1()$ is dominated by the value V_l^{i+1} at that point, it is simple to re-write the equation in terms of that variable and to evaluate it iteratively until converged.

5. Model testing, results and discussion

5.1. Experimental data

The ability of the proposed model to predict furrow advance, recession and runoff hydrograph was tested for 7 independent sets of furrow data. The selected tests covered a wide range of soil infiltration parameters, furrow lengths and field slopes. Five data sets were from experimental data available in the literature. Two of the field experiments were conducted under free drainage conditions during 2010 at the Isfahan University of Technology, Isfahan, Iran, Agricultural Research Farm (32°32′N, 51°23′E) on a bare sandy clay loam soil. The experiments were carried out on 45 m long furrows, spaced 0.75 m apart. The longitudinal slope of one field was 1.1% and the other was 2.9%. Average upstream inflow rate to each furrow was 0.7 L/s. One of the furrow data sets (Benson 2-2-1 furrow test) was reported by Elliott et al. (1982). The next furrow data set (Fort Morgan Farm, Colorado) was reported by Walker and Skogerboe (1987). Two furrow tests at the Karaj1 and Karaj2 Farm were reported by Abbasi et al. (2010). The Benson, Fort Morgan, Karaj1 and Karaj2 furrows were open ended furrows. The last data set was a blocked end furrow at Maricopa Agricultural Center reported by Abbasi et al. (2003).

Model simulations were carried out for estimating advance and recession trajectories, runoff volume and outflow hydrograph. For these simulations, the observed values of geometry of the furrow, furrow length, infiltration, upstream inflow discharge, and cut-off time were used as input parameters for each irrigation event. The bottom elevation data of each computational point in the furrow was interpolated by using linear or cubic-spline interpolation. Table 1 presents the input data sets used for testing the model performance. Several statistics were computed to assess the goodness-of-fit of the model. The root mean square error (RMSE) was used to compare measured and predicted advance/recession trajectory:

$$\mathrm{RMSE} = \sqrt{\frac{\sum_{i=1}^{N}(t_i' - t_i)^2}{N}} \quad (34)$$

where t_i' and t_i are predicted and measured values respectively of the advance or recession time and N is number of measurements.

The Nash–Sutcliffe efficiency (NSE) indicator was used to compare the measured and predicted runoff hydrographs:

$$\mathrm{NSE} = 1 - \frac{\sum_{i=1}^{N}(Q_i' - Q_i)^2}{\sum_{i=1}^{N}(Q_i' - \bar{Q})^2} \quad (35)$$

where Q_i' and Q_i are predicted and measured values respectively of the flow rate at the end of furrow, $\bar{Q}$ is the average of the measurements and N is number of measurements.

The net volumetric relative error (ε) was used to compare the measured and predicted total runoff volume at the end of the irrigation furrow:

$$\varepsilon = \frac{V_R' - V_R}{V_R} \quad (36)$$

where V_R' and V_R are predicted and measured values respectively of the total runoff volume.

5.2. Model validation

5.2.1. General

The accuracy of the proposed model in simulating various phases of furrow irrigation was evaluated by comparing the predicted advance, recession and outflow hydrographs with observed furrow data. Also, the accuracy of the proposed model was compared with the WinSRFR3.1 model. WinSRFR is an integrated hydraulic analysis application for surface irrigation systems that combines a simulation engine with tools for irrigation system evaluation, design, and operational analysis. WinSRFR is the successor to irrigation modeling software developed over the past 20 years by the USDA Agricultural Research Service (Bautista et al., 2009).

Water-surface profiles were simulated by Zero-inertia and Kinematic-wave solution engines of WinFRFR and Slow-change/slow-flow models at several different instants. The Manning resistance coefficient, used widely in surface irrigation literature, was computed from the proposed resistance model, Eqs. (13) and (14), at the advance and storage phases of the Slow-change/slow-flow model, to give an idea of the magnitude and variation along the furrows.

The performance of the WinSRFR model in simulating flow parameters is shown in Table 2 for the furrows tested. The performances of explicit and implicit methods for the Slow-change/slow-flow equation in simulating advance and recession times, runoff volumes and outflow hydrographs, and computational times (CPU) are presented in Tables 3 and 4.

5.2.2. Isfahan1 and Isfahan2 Farms

The simulated advance and recession times of the explicit and implicit solution of the Slow-change/slow-flow equation were in good agreement with the experimental data (Fig. 2). However, agreement was less satisfactory during the recession phase. The WinSRFR model also predicted advance and recession trajectories very similar to the Slow-change/slow-flow model. The differences in the RMSE indicators of advance and recession trajectories of the WinSRFR model (Table 2), explicit (Table 3) and

Table 1
Furrow modeling input data.

Model input parameter	Isfahan1	Isfahan2	Karaj1	Karaj2	Benson 2-2-1	Fort Morgan	Maricopa
Soil type	SCL	SCL	L	L	CL	LS	SL
Field length, L (m)	45	45	160	160	625	350	100
Furrow spacing, W (m)	0.75	0.75	0.75	0.75	1.52	1.5	1
Field slope, S_0 (m/m)	0.0290	0.0090	0.0054	0.0064	0.0040	0.0020	0.0001
Furrow geometry parameters							
C	1.329	1.411	1.532	1.532	1.105	0.652	2.058
m	0.546	0.563	0.612	0.612	0.366	0.212	0.638
Time of cutoff (min)	60	60	235	200	610	170	140
Infiltration parameters							
a	0.42	0.78	0.45	0.72	0.4	0.4	0.75
k ($m^3\ min^{-a}\ m^{-1}$)	0.00150	0.00098	0.00620	0.00180	0.00580	0.00347	0.00287
b ($m^3\ min\ m^{-1}$)	–		–		–	0.000325	–
Inflow rate, Q_0 (L/s)	0.70	0.70	1.41	0.89	1.17	2.76	1.26

Table 2
Goodness of fit of flow parameters for WinSRFR 3.1 model.

Parameter	Location						
	Isfahan1	Isfahan2	Karaj1	Karaj2	Benson 2-2-1	Fort Morgan	Maricopa
Advance times, RMSE (min)	0.3	0.7	1.8	4.1	4.2	5.1	2.36
Recession times, RMSE (min)	1.2	2.3	3.9	3.1	6	5.4	3.85
Runoff, NSE	0.94	0.89	0.65	0.93	0.8	0.74	–
Runoff volume, ε	0.42	−0.97	1.13	6.27	−9.42	−2.18	–

Table 3
Goodness of fit of flow parameters, space and time step and computational time for the explicit scheme.

Parameter	Location						
	Isfahan1	Isfahan2	Karaj1	Karaj2	Benson 2-2-1	Fort Morgan	Maricopa
Advance times, RMSE (min)	0.4	1.3	2.9	4.8	4.1	8.9	1.83
Recession times, RMSE (min)	2.0	2.1	6.5	4.5	6.0	6.8	2.58
Runoff, NSE	0.96	0.97	0.66	0.93	0.59	0.80	–
Runoff volume, ε	0.66	0.72	−2.49	12.00	−17.00	3.69	–
Δx (m)	2.5	2.5	10	10	25	25	4
Δt (s)	2	2	20	10	100	50	10
CPU (s)	45	48	19	23	15	20	

implicit (Table 4) solution of the Slow-change/slow-flow equation for Isfahan1 and Isfahan2 farms were minor. The runoff volume and general shape of the outflow hydrograph were well predicted by the explicit and implicit Slow-change/slow-flow model (Fig. 3). According to the NSE value and relative error, explicit and implicit Slow-change/slow-flow models were comparable with the WinSRFR model in predicting the runoff phase for Isfahan1 and 2 farms (Tables 2–4). The simulation time step for the implicit scheme was larger than for the explicit scheme. Therefore, the CPU time of the simulation for the implicit scheme was smaller than for the explicit scheme (Tables 3 and 4). The Zero inertia engine of WinSRFR gave sawtooth profiles for Isfahan1 and 2 furrows (Figs. 4a and 5a). They were eliminated for steep slopes by switching to Kinematic-wave models. WinSRFR switches the solution model from Zero-inertia to Kinematic-wave when the bottom slope exceeds 0.004 (USDA-ARS, 2009), as was the case for Isfahan1 (slope 0.029) and Isfahan2 (slope 0.009) furrows. Figs. 4b and 5b show that the water surface profiles of the Isfahan1 and Isfahan2 furrows are smooth with the Kinematic-wave model. The computed water surface profiles of the Slow-change/slow-flow model were also smooth. A constant Manning resistance of 0.03 and 0.05 was utilized in WinSRFR to simulate Isfahan1 and 2 furrows respectively. From Fig. 6a and b, it is observed that spatial variation of Manning's n in the advance phase (T3) was higher than the storage phase for those furrows. The average resistance coefficient at time TS along the furrow was 0.032 and 0.06 for Isfahan1 and 2 respectively. Therefore, the average

Table 4
Goodness of fit of flow parameters, space and time step and computational time for the implicit scheme.

Parameter	Location					
	Isfahan1	Isfahan2	Karaj1	Karaj2	Benson 2-2-1	Fort Morgan
Advance times, RMSE (min)	0.6	1	2.8	5.9	8.2	7.5
Recession times, RMSE (min)	1.1	2.7	4.1	4.1	7.8	5.1
Runoff, NSE	0.98	0.96	0.55	0.93	0.62	0.84
Runoff volume, ε	−0.14	0.27	−2.40	2.3	−9.2	−5.6
Δx (m)	2.5	2.5	10	10	25	25
Δt (s)	20	30	70	70	260	260
CPU (s)	10	8	12	8	10	6

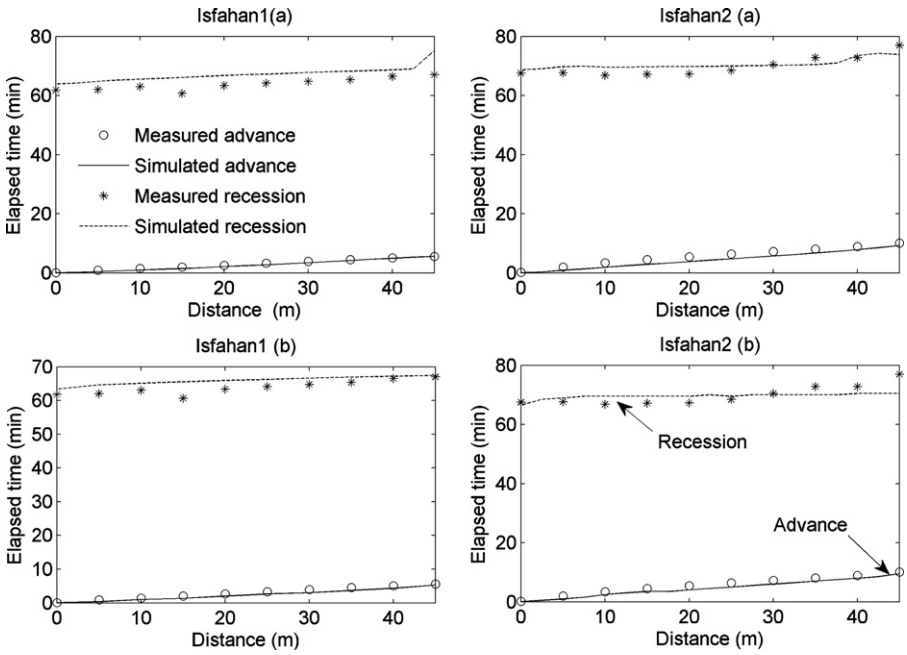

Fig. 2. Comparison of simulated and measured advance and recession trajectories for Isfahan1 and Isfahan2 farms using the Slow-change/slow-flow model. (a) Explicit scheme and (b) implicit scheme.

estimation of the proposed resistance model in the storage phase was comparable with the constant resistance coefficient applied in WinSRFR.

5.2.3. Karaj1 and Karaj2 Farms

Comparisons of the measured advance and recession trajectories with those predicted by the explicit and implicit Slow-change/slow-flow models are given in Fig. 7. The performance of the models in predicting advance and recession trajectories of Karaj1 and Karaj2 farms was good. The evaluation of goodness of fit parameters showed that WinSRFR and Slow-change/slow-flow models produced comparable values for Karaj1 and Karaj2 farms (Tables 2–4). The RMSEs of advance and recession trajectories of the Slow-change/slow-flow model for Karaj1 and Karaj2 farms were higher than the WinSRFR model, but discrepancies were not significant (Tables 2–4). The Slow-change/slow-flow model simulated the runoff phase of Karaj1 and 2 farms with a fair degree of accuracy (Fig. 8). According to the NSE value and relative error, the explicit and implicit Slow-change/slow-flow models were comparable with the WinSRFR model in predicting of the runoff phase for Karaj1 and Karaj2 farms, although the relative error of the implicit scheme in prediction of runoff volume was less than the Euler explicit scheme (Tables 2–4). Using the implicit instead of the explicit scheme decreased CPU time, as it allowed larger

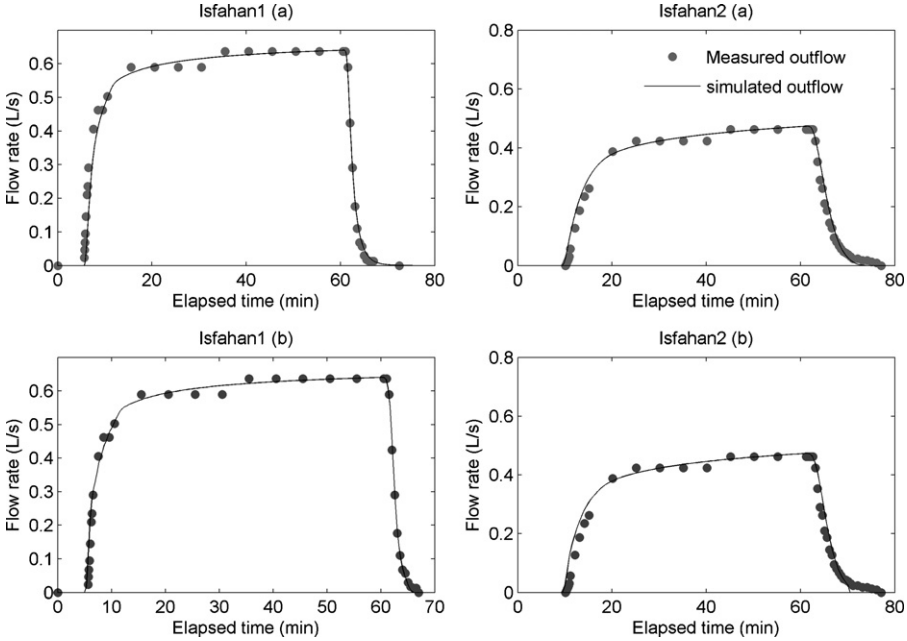

Fig. 3. Comparison of simulated and measured outflow hydrograph (runoff) for Isfahan1 and Isfahan2 farms using the Slow-change/slow-flow model. (a) Explicit scheme and (b) implicit scheme.

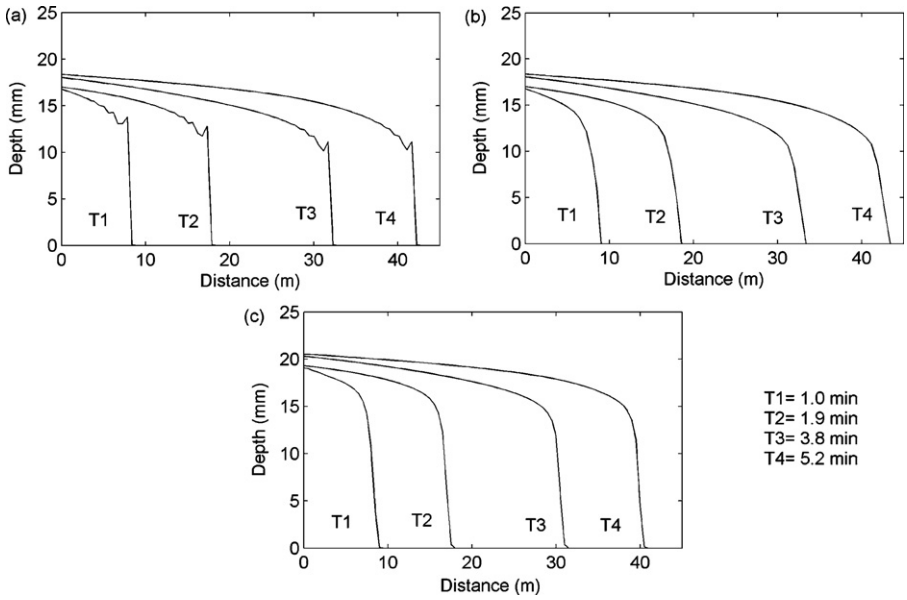

Fig. 4. Comparison of water surface profiles for Isfahan1 furrow by: (a) Zero-inertia engine of WinSRFR, (b) Kinematic-wave engine of WinSRFR and (c) Slow-change/slow-flow model.

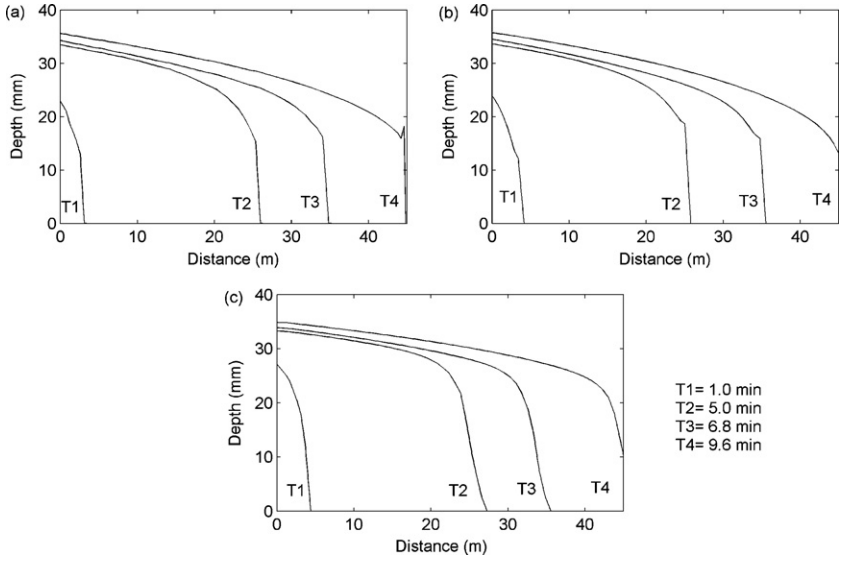

Fig. 5. Comparison of water surface profiles for Isfahan2 furrow by: (a) Zero-inertia engine of WinSRFR, (b) Kinematic-wave engine of WinSRFR and (c) Slow-change/slow-flow model.

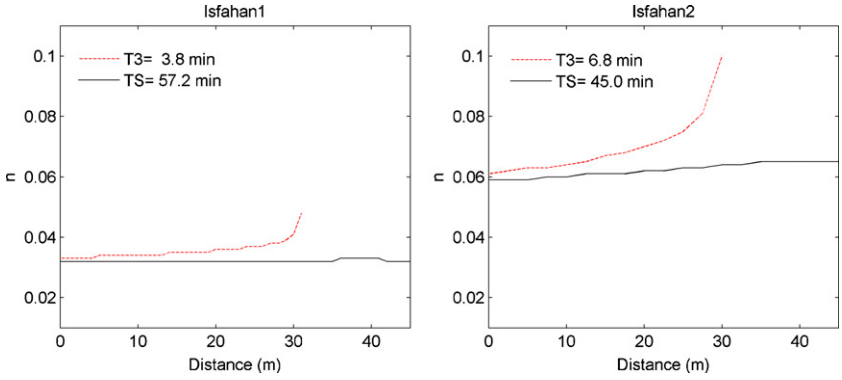

Fig. 6. Spatial variation of the derived Manning's *n* from the proposed resistance model at two different instants for Isfahan1 and Isfahan2 furrows.

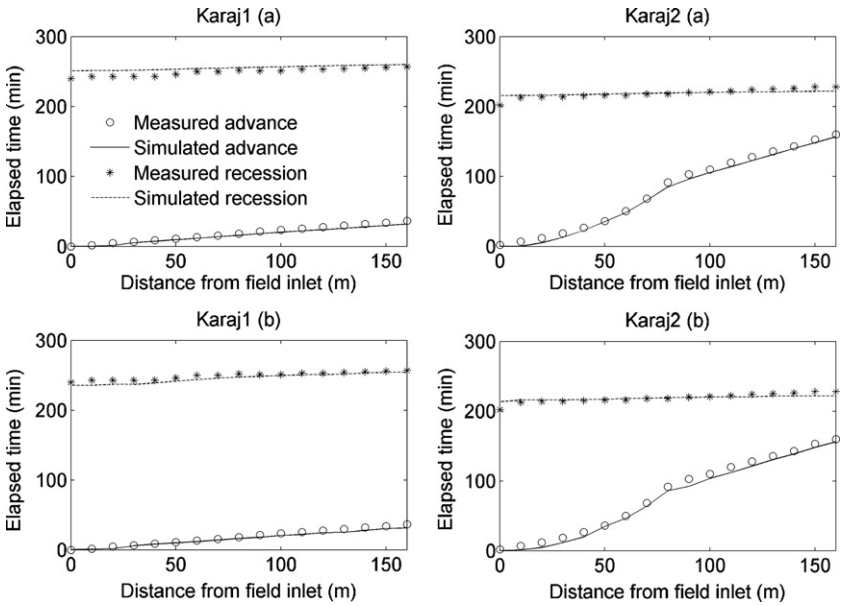

Fig. 7. Comparison of simulated and measured advance and recession trajectories for Karaj1 and Karaj2 farms using the Slow-change/slow-flow model. (a) Explicit scheme and (b) implicit scheme.

time steps. The bottom slope of Karaj1 (0.005) and Karaj2 (0.006) furrows was slightly greater than 0.004. Therefore, the computed fourth Zero-inertia water surface profile (T4) had a sawtooth shape for Karaj1 and 2 furrows (Figs. 9a and 10a). Figs. 9b and 10b show that the water surface profiles of Karaj1 and Karaj2 furrows were smooth with the Kinematic-wave model. The Slow-change/slow-flow simulated water surface profiles (Figs. 9c and 10c) were comparable with the Kinematic-wave simulated surface profiles (Figs. 9b and 10b) for Karaj1 and 2 furrows, respectively. A constant Manning coefficient of 0.045 and 0.08 was utilized to simulate Karaj1 and 2 furrow irrigations respectively by WinSRFR. From Fig. 11a and b it is observed that the spatial variation of Manning's *n* in the advance phase (T3) was higher than the storage phase (TS) for Karaj1 and Karaj2 furrows. The average resistance coefficient at time TS along the furrow was 0.05 and 0.085 for Karaj1 and 2 respectively. Therefore, the average estimation of the proposed resistance model in the storage phase was comparable with the constant resistance coefficient applied in WinSRFR.

5.2.4. Benson 2-2-1 and Fort Morgan

The simulated advance and recession trajectories of the explicit and implicit Slow-change/slow-flow models for Benson and Fort Morgan farms compared very well with measured values as shown in Fig. 12. The WinSRFR model also predicted advance

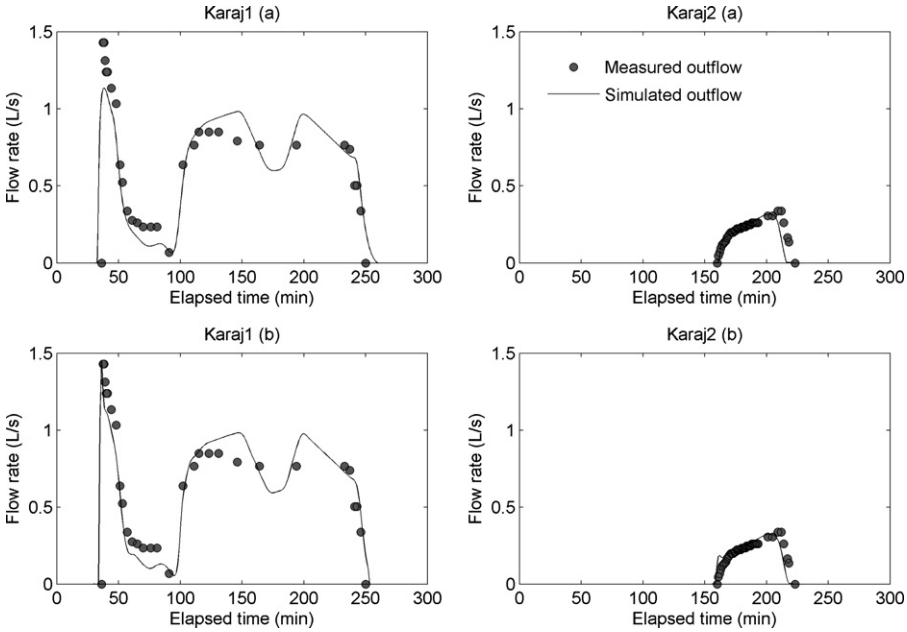

Fig. 8. Comparison of simulated and measured outflow hydrograph (runoff) for Karaj1 and Karaj2 using the Slow-change/slow-flow model. (a) Explicit scheme and (b) implicit scheme.

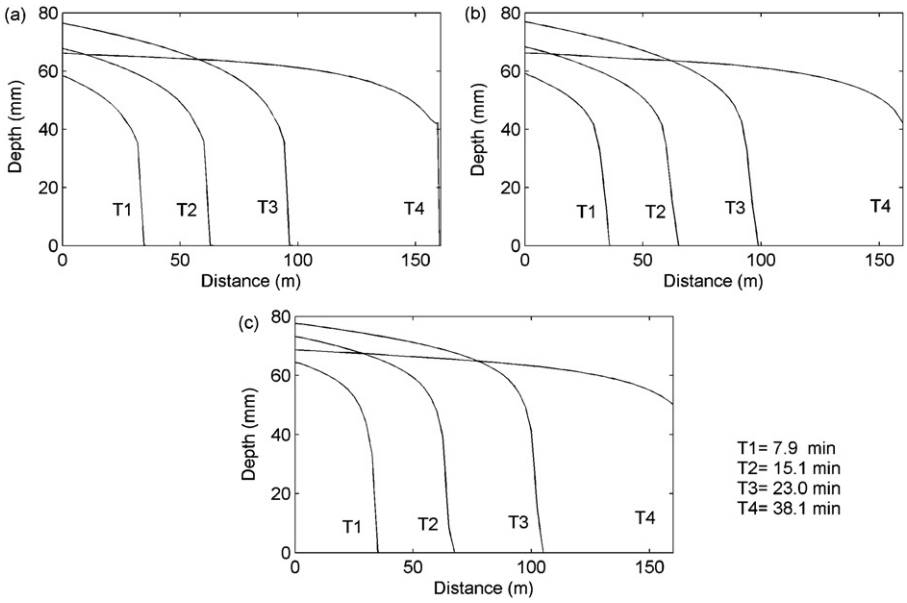

Fig. 9. Comparison of water surface profiles for Karaj1 furrow by: (a) Zero-inertia engine of WinSRFR, (b) Kinematic-wave engine of WinSRFR and (c) Slow-change/slow-flow model.

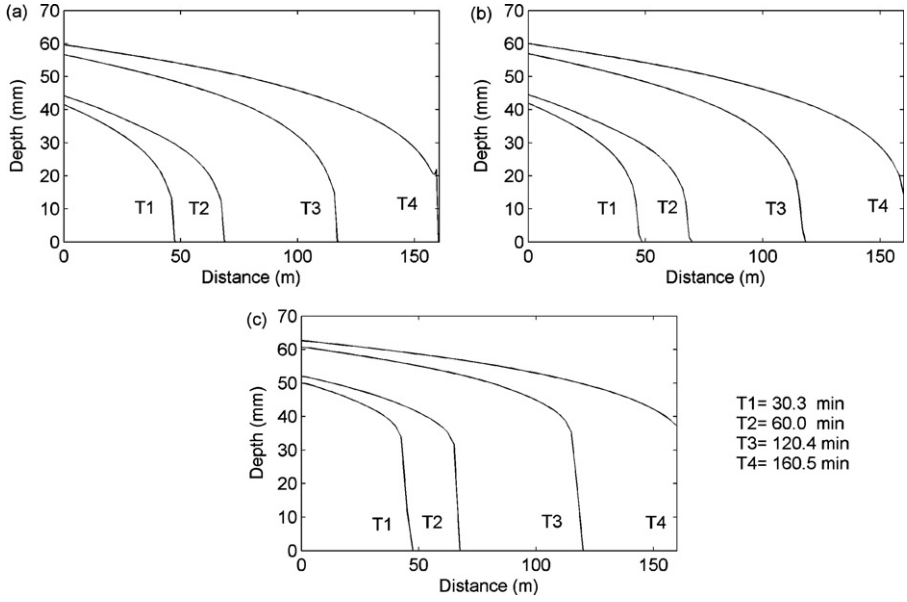

Fig. 10. Comparison of water surface profiles for Karaj2 furrow by: (a) Zero-inertia engine of WinSRFR, (b) Kinematic-wave engine of WinSRFR and (c) Slow-change/slow-flow model.

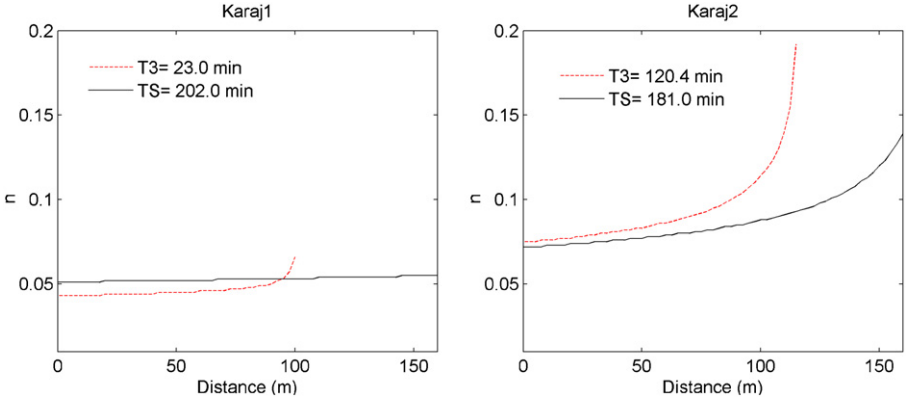

Fig. 11. Spatial variation of the derived Manning' *n* from the proposed resistance model at two different instants for Karaj1 and Karaj2 furrows.

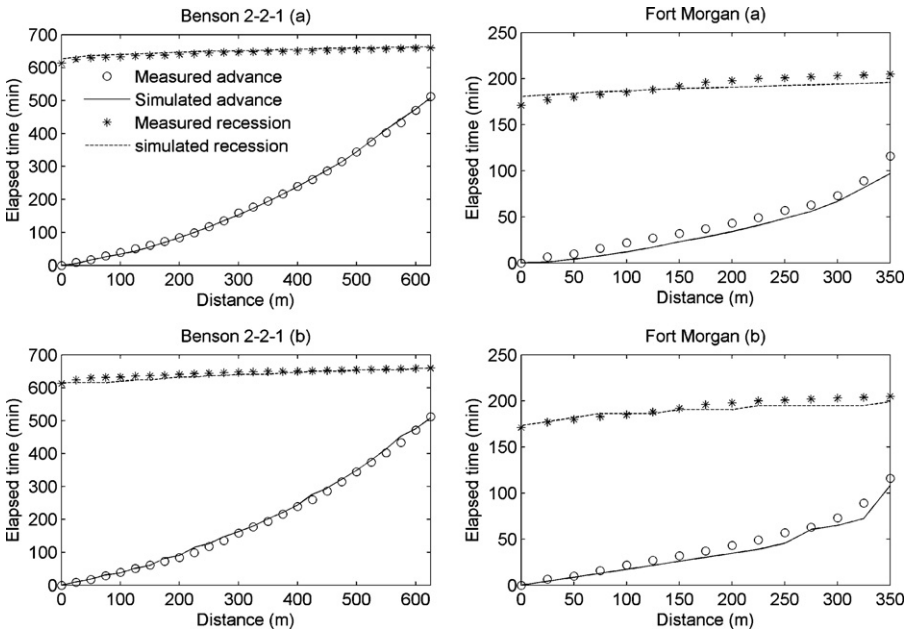

Fig. 12. Comparison of simulated and measured advance and recession trajectories for Benson 2-2-1 and Fort Morgan farms using the Slow-change/slow-flow model. (a) Explicit scheme and (b) implicit scheme.

and recession trajectories very similar to those of the Slow-change/slow-flow model. The differences in the RMSE indicators of advance and recession trajectories of the WinSRFR model (Table 2) and the explicit (Table 3) and implicit (Table 4) solution of the Slow-change/slow-flow equation for Benson and Fort Morgan farm were small. The model simulated the runoff phase of Benson and Fort Morgan farms with a fair degree of accuracy (Fig. 13). According to the NSE value and relative error, the explicit and implicit Slow-change/slow-flow models were comparable with WinSRFR model in predicting the runoff phase for Benson and Fort Morgan farms (Tables 2–4). The simulation time step for the implicit scheme was larger than for the explicit scheme so that the CPU time of simulation for the implicit scheme was again smaller than for the explicit scheme (Tables 3 and 4). The bottom slope of Benson furrow was about 0.0042. As expected, Zero-inertia computed water surface profiles for this furrow have a sawtooth shape (Fig. 14a). The Kinematic-wave (Fig. 14b) and Slow-change/slow-flow (Fig. 14c) models were applied, with water surface profiles similarly smooth for the Benson furrow. The bottom slope of the Fort Morgan furrow was about 0.002, but the Kinematic-wave model is not recommended for use with mild slopes (USDA-ARS, 2009). The simulated water surface profiles of the Slow-change/slow-flow (Fig. 15b) model were comparable with Zero-inertia surface profiles (Fig. 15a) for the Fort Morgan furrow.

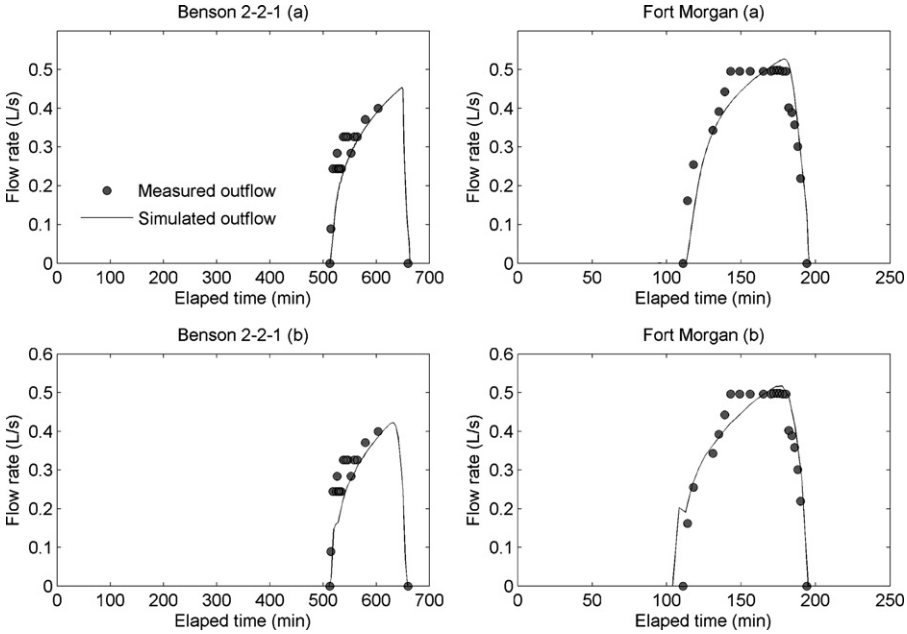

Fig. 13. Comparison of simulated and measured outflow hydrograph (runoff) for Benson 2-2-1 and Fort Morgan farms using the Slow-change/slow-flow model. (a) Explicit scheme and (b) implicit scheme.

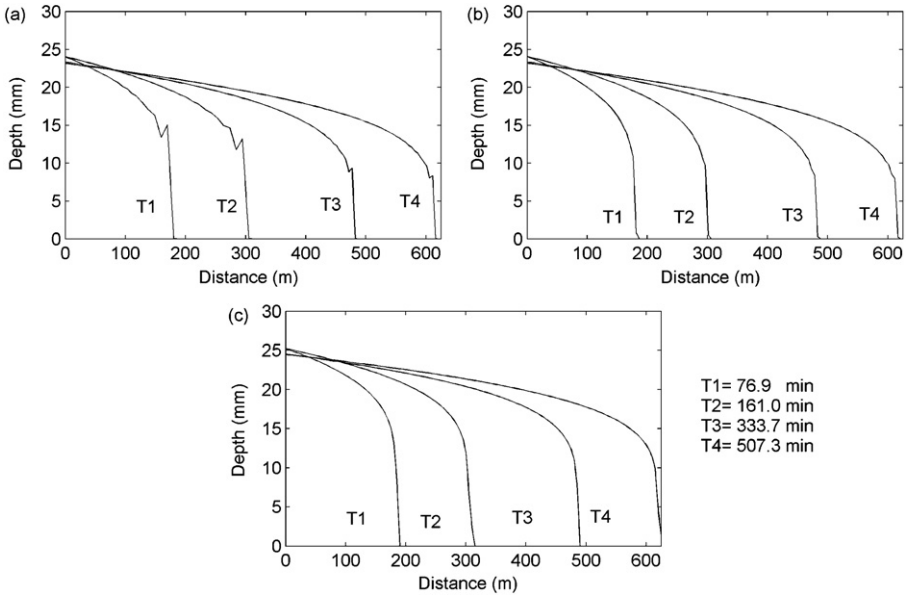

Fig. 14. Comparison of water surface profiles for Benson 2-2-1 furrow by: (a) Zero-inertia engine of WinSRFR, (b) Kinematic-wave engine of WinSRFR and (c) Slow-change/slow-flow model.

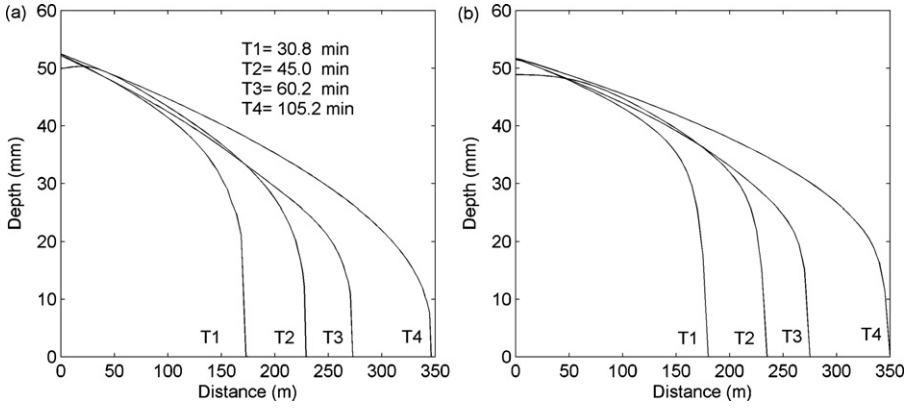

Fig. 15. Comparison of water surface profiles for Fort Morgan furrow by: (a) Zero-inertia engine of WinSRFR, (b) Slow-change/slow-flow model.

A constant Manning resistance coefficient of 0.02 and 0.04 was utilized to simulate Benson and Fort Morgan furrow irrigations by WinSRFR, respectively. From Fig. 16a and b, it is observed that the spatial variation of Manning's n in the advance phase (T3) was higher than the storage phase (TS) for both furrows. The average resistance coefficient at time TS along the furrow was 0.021 and 0.045 for those furrows, respectively. Therefore, the average estimation from the proposed resistance model in the storage phase

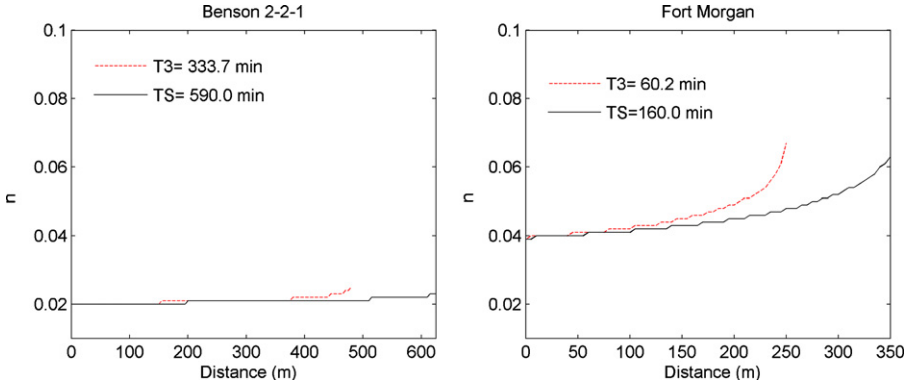

Fig. 16. Spatial variation of the derived Manning' n from the proposed resistance model at two different instants for Benson and Fort Morgan furrows.

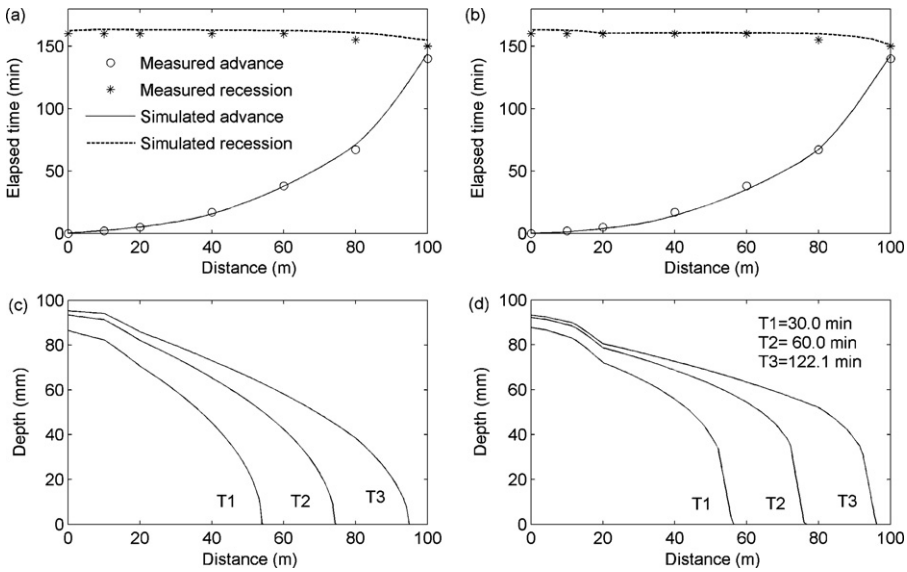

Fig. 17. The simulated and measured advance and recession trajectories for Maricopa furrow by: (a) Zero-inertia engine of WinSRFR, (b) Slow-change/slow-flow model; and simulated water surface profiles for Maricopa furrow by: (c) Zero-inertia engine of WinSRFR, (d) Slow-change/slow-flow model.

was comparable with the constant resistance coefficient applied in WinSRFR.

5.2.5. Maricopa

The simulated advance and recession trajectories of the Slow-change/slow-flow models for the Maricopa blocked-end furrow compared very well with measured values as shown in Fig. 17b. The WinSRFR model also predicted advance and recession trajectories very similar to the Slow-change/slow-flow model (Fig. 17a). The differences in the RMSE indicators of advance and recession trajectories of the WinSRFR model (Table 2) and explicit solution of Slow-change/slow-flow equation (Table 3) for the Maricopa furrow were small. The Kinematic-wave model is not applicable in blocked end furrows. The simulated water surface profiles of the Slow-change/slow-flow (Fig. 17d) model were comparable with the Zero-inertia surface profiles (Fig. 17c). A constant Manning resistance coefficient of 0.073 was utilized to simulate Maricopa furrow irrigation by WinSRFR. Fig. 18 shows spatial variation of Manning's n in the advance phase (T3). The water front arrived at the end of the Maricopa furrow at cutoff time. Therefore, depletion was started immediately after the end of the advance phase. The average resistance coefficient at cutoff time along the Maricopa furrow was 0.068.

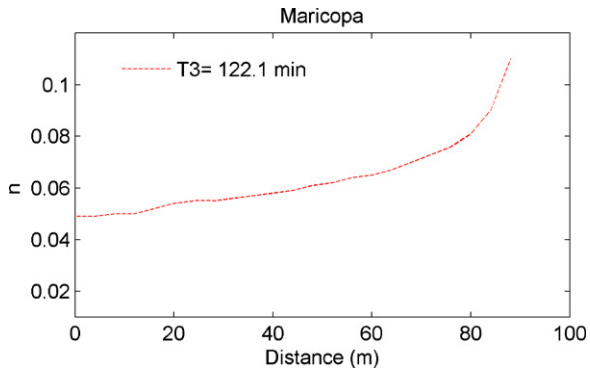

Fig. 18. Spatial variation of the derived Manning's n from proposed the resistance model at one instant in the advance phase.

5.3. Comparison of present method with Zero-inertia model

In our computations we generally found that there was a good agreement between the results from our Slow-change/slow-flow model and those from WinSRFR. However, there are some comparisons of a theoretical and computational nature that can be made:

- The two models use the same simplified momentum equation. However, we believe that its chief approximation, the neglect of two terms in the long-wave momentum equation, is that rates of change in the boundary conditions, and hence in the channel, are small, and not because inertia effects are small. We have presented some results of calculations where the steady form of the equation was used to calculate successfully flows over free overfalls where the flows were sub-, trans-, and even super-critical, supporting our conjecture.
- The Zero-inertia model uses two equations in terms of two variables, discharge and water depth, and updates them with the two conservation equations, one being exact, mass conservation, and the other the approximate momentum equation. The Slow-change/slow-flow model connects the two variables using the concept of upstream volume, which is used with the approximate momentum equation to give a single equation with a single unknown. In itself, this is not an important difference between the two models.
- There is a difference between the two models in the provision of boundary conditions at the upstream boundary. The Zero-inertia model uses an approximation based on mean slope in the channel (e.g. Eq. (12) of Bautista et al., 2009), although it would be possible to use the mass-conservation equation at the upstream boundary to give a value of $\partial h/\partial t$ that could be used in time-stepping. Our use of upstream volume requires only the inflow hydrograph at the boundary, although a consequence of our formulation is that the instantaneous inflow there actually appears in the differential equation, which in computations is a minor feature, as at a particular time step it has the same numerical value for all points.
- The computational technique using Zero-inertia seems to be more complicated, involving a variable domain and linearization of the equations (Strelkoff and Katopodes, 1977a; Elliott et al.,

1982). Strelkoff and Katopodes (1977a) stated that the linearization could have provided the basis for an iterative method, but thought it unnecessary. The computational methods developed here use conventional finite differences (occasionally enhanced by splines). The simplest method used explicit fully non-linear time-stepping, while the implicit method also required linearization of the non-linear equations for solution (more simply done here by numerical differentiation) but the iteration process was continued here, thereby providing non-linear solutions. A simpler variant of that method, not reported above, used direct iteration to solve the non-linear equation at each point.

- In the computations reported here, we had to start with a thin stream of 2 mm depth, as in other computations with a similar equation (Barlow et al., 2006).
- The composite formula (13) for resistance coefficient λ in terms of Depth/Roughness and Eq. (14) for n could be used as an estimate in any channel computational method. As they are also applied for very small depths provided Depth/Roughness $(A/W_p)/d_{84} \geq 0.26$, they are particularly useful for computations involving the commencement of irrigation.

6. Conclusions

A furrow irrigation model was developed, based on the Slow-change/slow-flow routing equation, a single equation which is a reduced form of the Saint-Venant equations. The approximate momentum equation used is the same as the Zero-inertia approximation, but here it is asserted that the approximation lies in the relative slowness of change of boundary conditions and not in smallness of the Froude number. In apparent violation of that, in furrow irrigation problems, inflow can be changed suddenly, but there is some evidence that this has little effect on results. Introducing the concept of upstream volume gives a routing equation with a single variable, with convenient incorporation of upstream, downstream, and open boundary conditions. For resistance to flow a model is proposed in terms of arbitrary boundary roughness using a combination of two existing models. Infiltration is assumed to follow the Kostiakov formula. The model was solved numerically using the explicit Euler and implicit Crank–Nicolson schemes. The accuracy of the model was demonstrated with a range of field conditions and could simulate all phases of the irrigation process. The performance was compared with the WinSRFR model. In all cases examined, the proposed model provided predictions that were in good agreement with field data and the WinSRFR model results. What has not been examined here is the accuracy of the model compared with a full hydraulic model. The Slow-change/slow-flow routing model is capable of simulating water surface profiles for a wide range of boundary conditions, both inflow and outflow (or no outflow), without unnecessary extra approximations, and for relatively mild slope and relatively steep slope furrows without showing sawtooth profiles. It appears to be a promising tool as it eliminates the need for separate models for different conditions. It provides a suitable and simple numerical simulation tool for design and evaluation of furrow irrigation.

Acknowledgements

The authors would like to thank the Isfahan University of Technology for financial support and Prof. P. Tschernutter and the Vienna University of Technology Institute of Hydraulic Engineering and Water Resources for hosting F. Soroush for six months.

References

Abbasi, F., Adamsen, F.J., Hunsaker, D.J., Feyen, J., Shouse, P., van Genuchten, M.Th, 2003. Effects of flow depth on water flow and solute transport in furrow irrigation: field data analysis. Journal of Irrigation and Drainage Engineering 129 (4), 237–246.

Abbasi, F., Taefeh-Rezaie, H., Jalini, M., 2010. The possibility of fertigation in different furrow irrigation regimes. Tech. Rep., No. 523. Agricultural Engineering Research Institute, Karaj, Iran.

Barlow, K., Fenton, J.D., Nash, D., Grayson, R., 2006. Modelling phosphorus transport in a surface irrigation drain. Advances in Water Resources 29 (9), 1383–1398.

Bassett, D.L., Fitzsimmons, D.W., 1976. Simulation overland flow in border irrigation. Transactions of the ASAE 19 (4), 666–671.

Bautista, E., Clemmens, A.J., Strelkoff, T.S., Schlegel, J., 2009. Modern analysis of surface irrigation systems with WinSRFR. Agricultural Water Management 96, 1146–1154.

Beirami, M.K., Nabavi, S.V., Chamani, M.R., 2006. Free overfall in channels with different cross sections and sub-critical flow. Iranian Journal of Science & Technology, Transaction B, Engineering 30 (B1), 97–105, http://www.scribd.com/doc/68125481/Beirami-30B1.

Burguete, J., Zapata, N., García-Navarro, P., Maïkaka, M., Playán, E., Murillo, J., 2009. Fertigation in furrows and level furrow systems. I: model description and numerical tests. Journal of Irrigation and Drainage Engineering 135 (4), 401–412.

De Boor, C., 1978. A Practical Guide to Splines. Springer, New York.

Elliott, R.L., Walker, W.R., Skogerboe, G.V., 1982. Zero-inertia modeling of furrow irrigation advance. Journal of Irrigation and Drainage Engineering – ASCE 108 (3), 179–195.

Fangmeier, D.D., Strelkoff, T., 1979. Mathematical models and border irrigation design. Transactions of the ASAE 22 (1), 93–99.

Fenton, J.D., 2012. Long waves in open channels – their nature, equations, approximations, and numerical simulation. Alternative Hydraulics Report 5. http://johndfenton.com/Papers/05-Long-waves-in-open-channels.pdf.

Fenton, J.D., Keller, R.J., 2001. The calculation of streamflow from measurements of stage. Tech. Rep. 01/6, Cooperative Research Centre for Catchment Hydrology, Melbourne. http://www.catchment.crc.org.au/pdfs/technical200106.pdf.

Fenton, J.D., Oakes, A.M., Aughton, D.J., 1999. On the nature of waves in canals and gate stroking and control. In: Proceeding Workshop on Modernization of Irrigation Water Delivery Systems, US Committee on Irrigation and Drainage, Phoenix, Arizona, October 17–21, pp. 343–357, http://johndfenton.com/Papers/Fenton99Phoenix-On-the-nature-of-waves-in-canals-and-gate-stroking-and-control.pdf.

Guo, J., 2002. Logarithmic matching and its applications in computational hydraulics and sediment transport. Journal of Hydraulic Research 40, 555–565.

Kennedy, J.F., Macagno, E.O., 1971. Selected Writings of Hunter Rouse. Dover.

Kostiakov, A.V., 1932. On the dynamics of the coefficient of water percolation in soils and on the necessity for studying it from a dynamics point of view for the purposes of amelioration. In: Transactions of the 6th Commission of the International Society of Soil Science, America, pp. 17–21.

Merriam, J.L., Keller, J., 1978. Farm Irrigation System Evaluation: A Guide for Management. Agricultural and Irrigation Engineering Department, Utah State University, Logan, UT.

Pagliara, S., Das, R., Carnacina, I., 2008. Flow resistance in large-scale roughness condition. Canadian Journal of Civil Engineering 35 (11), 1285–1293.

Sherman, B., Singh, V.P., 1982. A kinematic model for surface irrigation: an extension. Water Resources Research 18 (3), 659–667.

Strelkoff, T.S., Clemmens, A.J., 2000. Approximating wetted perimeter in power-law cross section. Journal of Irrigation and Drainage Engineering 126 (2), 98–109.

Strelkoff, T.S., Katopodes, N.D., 1977a. Border irrigation hydraulics with zero-inertia. Journal of Irrigation and Drainage Engineering – ASCE 103 (HY3), 325–342.

Strelkoff, T.S., Katopodes, N.D., 1977b. End depth under zero-inertia conditions. Journal of the Hydraulics Division 103 (HY7), 699–711.

Thomas, L.H., 1949. Elliptic problems in linear difference equations over a network. Report of Watson Science Computing Laboratory, Columbia University, New York.

USDA-ARS (US Department of Agriculture, Agricultural Research Service), 2009. WinSRFR Version 3.1 User Manual. U.S. Arid Land Agricultural Research Center, Maricopa, AZ.

Walker, W.R., Humpherys, A.S., 1983. Kinematic-wave furrow irrigation model. Journal of Irrigation and Drainage Engineering 109 (4), 377–392.

Walker, W.R., Skogerboe, G.V., 1987. Surface Irrigation: Theory and Practice. Prentice-Hall Inc., Englewood Cliffs, NJ.

Yen, B.C., 1991. Hydraulic resistance in open channels. In: Yen, B.C. (Ed.), Channel Flow Resistance: Centennial of Manning's Formula, Highlands Ranch. Water Resource Publications, USA, pp. 1–135.